Y. M. Zhang
Mem. ASME

R. Kovacevic
Mem. ASME

Center for Robotics and Manufacturing Systems and Department of Mechanical Engineering, University of Kentucky, Lexington, KY

L. Wu
National Key Laboratory for Advanced Welding Production, Harbin Institute of Technology, Harbin, China

Dynamic Analysis and Identification of Gas Tungsten Arc Welding Process for Weld Penetration Control

In this study, gas tungsten arc welding is analyzed and modeled as a 2-input (welding current and arc length) 2-output (weld depression and width) multivariable process. Experiments under a number of typical welding conditions are performed to excite and identify the process characteristics and variations. It is observed that the model parameters vary in a large range with the experimental conditions. A real-time model frame with only a few parameters to be identified on-line is proposed. Based on the obtained models, the process characteristics in terms of inertia, delay, nonminimum phase, and coupling are given. These characteristics suggest an adaptive predictive decoupling control algorithm. By designing and implementing the suggested control algorithm with the real-time model, excellent results have been achieved for both simulation and practical control. This shows that the dynamic analysis and identification provide sufficient process information for design of the control system.

1 Introduction

Back-side weld width and penetration depth are major factors in the final weld quality for full penetration and partial penetration, respectively. Their sensing and control are critical and challenging issues in automated welding. Although extensive research has been done to find feasible approaches for sensing these parameters using top-side sensors, more practical solutions are still strongly needed for different cases. In an effort towards a novel top-side sensing approach, we found that the back-side bead width can be monitored utilizing the top-side weld width and depression in gas tungsten arc welding (GTAW) [1]. Thus, a vision-based system can be developed to sense and control the weld penetration.

To complete the corresponding control system, the characteristics of the GTAW process must be analyzed and modeled accordingly. The acquired process characteristics can be employed to select the control algorithm. The resultant models will be directly used in control algorithm design and implementation. Thus, dynamic analysis and identification play important roles in the corresponding control system design.

Numerical simulation has been an important tool to study the characteristics of arc welding processes [2–9]. It is different from the dynamic identification which will be performed in this study. For numerical simulation, different process parameters from temperature field, weld pool geometry to weld pool fluid are computed from the given input parameters. The major objective seems to be the open-loop prediction of the welding process for the process understanding and welding parameter selection. The model cannot be changed on-line using the measured feedback innovation. The calculation is done prior to the welding. No real-time computation is required. Exact knowledge of welding condition is assumed. In closed-loop control, undescribed welding condition variation is a fundamental assumption. The resultant variations in the process (output) parameters are overcome by adjusting the input parameters. In this case, especially for the predictive controls [10, 11], the model will be used for real-time computation. Real-time model modification using the feedback may also be required. Thus, the corresponding requirement of the process model is distinct from the numerical simulation. Also, the concern of the process knowledge is different. For example, delay, i.e., the dead-time [12], and nonminimum phase [13] may be of concern. However, for the numerical simulation studies, no such topics have been addressed.

It should be pointed out that the dynamic identification and control of arc welding processes have been explored through a number of studies. In addition to the conventional PID control [14], advanced control techniques such as the optimal control [15] and adaptive control [16–18, 10] have also been used to generate sound welds. In the optimal control [15], the dynamic model of the arc welding process is off-line identified prior to the welding. To eliminate the influence of variations in welding conditions, the welding process model can be identified on-line for adaptive control. The standard recursive least squares algorithm has been used to estimate the model parameters [18]. In most cases, the arc welding processes can be modeled using lower order models [18, 10], and the accuracy of the modified model is sufficient for the adaptive controls. In these studies, no substantial feedback delays were encountered. The requirement on the modeling is, therefore, not as high as when a substantial delay exists. In this study, the objective is the top-side sensing-based control of the weld penetration, rather than the back-side sensing-based control [18]. An increased feedback delay is encountered [1]. (Also, the delay depends on the welding conditions.) The resultant requirement on the modeling is higher. In order to meet this higher requirement, a detailed analysis is performed to understand the characteristics of the process. Based on the analysis and modeling experimentation, a real-time model frame is proposed to combine the general characteristics of the process with a few adjustable critical parameters which can be on-line identified with sufficient accuracy during a short welding duration. Also, the well-known generalized predictive control has been used instead of the conventional adaptive control algorithms in order to improve the robustness of the resultant control system. This algorithm has been widely accepted as an excellent robust adaptive control for different processes with varied order, delay, parameters, and non-minimum-phase as encountered in this study [19–22]. Consequently, a qualified system can be developed to control the full

Contributed by the Manufacturing Engineering Division for publication in the JOURNAL OF ENGINEERING FOR INDUSTRY. Manuscript received May 1994; revised Nov. 1994. Associate Technical Editor: E. Kannatey-Asiba, Jr.

penetration using the proposed top-side sensor based on the analysis and dynamic modeling.

2 Process

The addressed control system is described in Fig. 1. The weld depression h and weld width b, defined in Fig. 2, can be computed from the laser stripe. The required full penetration state is produced by controlling h and b. Thus, h and b are the outputs of the addressed control process. They can be adjusted by changing the welding parameters. These welding parameters are the process inputs, i.e., the control variables.

It is well known that thermal and force parameters of a welding process depend to a great extent on torch velocity, welding current and arc length (or arc voltage). Also, both the depression h and the weld width b are dominated by the thermal and force parameters. Thus, h and b can be changed by adjusting the velocity, welding current and arc length. For a human operator, real time control of the penetration state is realized by adjusting the velocity and arc length during welding, while maintaining a constant welding current. It is, however, more convenient to change the current and arc length in real time in the case of either robotic welding or automatic welding, using the preprogrammed torch velocity. In fact, once the operating point (i.e., the bases of control variables around which the practical values of control variables vary in a certain range during real time control) is set, the effect of a small adjustment in velocity on the process can be achieved by changing both arc length and welding current. (The major effect of a change of velocity is in the power density of the heat source, and the latter can be fully controlled by arc length and welding current [23].) As a result, the welding current and arc length are selected to be the control variables. Thus, the addressed process is the gas tungsten arc welding process where (h, b) are controlled by adjusting (i, l). This is a two-input/two-output process.

2.1 Disturbances. In principle, a negative feedback control tends to adjust the outputs to the desired values. However, in order to acquire better control performance, the feedback control algorithm must be determined by the characteristics of the process to be controlled. The process model which correlates the process output with the control variable is a mathematical description of the process characteristics. It is evident that for any welding process, the process model may vary with application case. (For example, for different material and material thickness, different weld pool size or thermal field will be produced using the same welding parameters.) It is important to clearly describe the application case before the process analysis and model identification are performed. In this study, application case is described by the basic welding condition and disturbance.

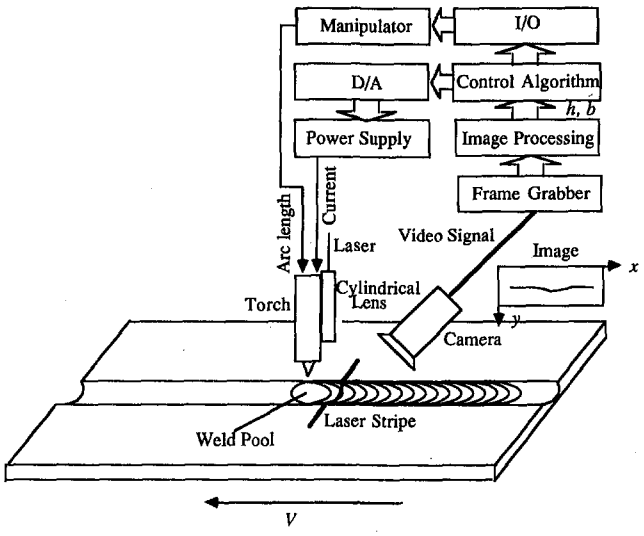

Fig. 1 Experimental system diagram. The sensor, which consists of the laser, lens, and camera, is attached to and moves with the torch.

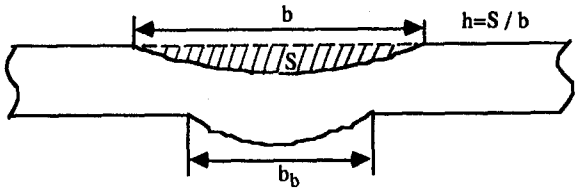

Fig. 2 Full penetration weld parameters. This is a cross section of a full penetration weld. *S* is the cross section area of the depression, *b* is the top-side weld width. The weld depression *h* is defined as the ratio *h* = *S*/*b*. It can be seen that *h* is actually the average weld depression of the cross section.

For any specific application, certain welding parameters can be assumed to be constant during welding and from case to case. Some may vary during welding or from case to case. For example, the thickness of the material may be considered as constant. Butt gap may vary during welding. Electrode tip angle may vary from time to time. Also, of the varied welding parameters, some may fluctuate around the basic values and some may exhibit random variation. In this study, the constants and the basic values are considered as the basic welding conditions. The varied parameters or portions are regarded as the process disturbances. The objective of welding process control is to overcome the influence of the disturbances on the concerned process outputs, under the basic welding conditions.

The basic welding conditions and the disturbances should be determined based on practical information. We assume that the torch velocity, three dimensions of the weldment, diameter of the electrode, material of the weldment and welding position are given. We further assume that the joint gap, electrode tip angle, heat transfer condition and flow rate of shielding-gas vary about the respective basic values. Thus, the given conditions and the aforementioned basic values are our basic welding conditions and any variations about the basic values are disturbances. The process models will be acquired by adding disturbances to the basic welding conditions.

2.2 Time Constants. Time constant is an important parameter to describe the characteristics of a dynamic process. For our 2input-2output process, there are four types of time constants: depression h to welding current i, depression h to arc length l, weld width b to welding current i, weld width b to arc length l. All of the time constants depend on the velocity, welding current, arc length, thickness of weldment, material of base metal, welding position, and so on. When the velocity, thickness and material are given, if the welding current, arc length and welding position vary within a small range, the time constants will not change greatly. Thus, under given welding conditions, it is feasible to obtain preliminary estimates of the time constants by experiments.

It is shown by step response experiments [24] that the time constant is about 4 seconds for h to i, about 1 second for h to l, about 2 seconds for b to i, and about 1 second for b to l. The time constant of depression to welding current is the dominant time constant (about 4 seconds). Due to the unneglectable time constants, the process is fundamentally dynamic.

2.3 Effect Intervals and Characteristics. Figure 3 shows a top view of weld pool region at a moment where: (1) z_0: the center of electrode, (2) z_1: the end of weld pool where the depression is just fixed, (3) z_2: the position where the weld pool is the widest and the weld width is just fixed, and (4) z_3: the position where the laser stripe lies. From z_3 to z_0,

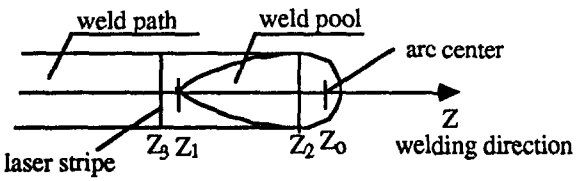

Fig. 3 Top view of weld pool region. This top-view shows the position relationship among the arc, weld pool, and laser strip.

the distance is 20 millimeters. And at this position, both h and b are extracted by processing the weld image illuminated by a laser stripe.

From Fig. 3 it is observed that the arc at z_0 can affect the weld width backward until z_2 and the depression backward until z_1. Therefore, the weld width at z_0 can be affected by the arc forward until $(z_0 + (z_0 - z_2))$. Similarly, the depression at z_0 can be affected by the arc forward until the point $z_0 + (z_0 - z_1)$. Let us define the effect interval as the distance along the welding direction for which the arc can affect either the depression or the weld width.

Suppose the effect interval of the arc on weld width at z_0 is $(z_0^{(2)}, z_0 + (z_0 - z_2))$ and the effect on depression is $(z_0^{(1)}, z_0 + (z_0 - z_1))$. In general, $z_0^{(2)} < z_0$, $z_0^{(1)} < z_0$. By analysis, the arc position where it produces its maximum effect on the weld parameters formation at z_0 is not z_0, but some place ahead of z_0 along the Z axis. Moreover, when the arc travels to position $z_0 + (z_0 - z_1)$, the depression at z_0 is almost fixed. Therefore, the effect of the arc at this position on the depression at z_0 is almost zero. Similarly, to the arc at $z_0 + (z_0 - z_2)$, its effect on the weld width at z_0 is also almost zero. Therefore, the effects of arc on the weld width and the depression at z_0 versus the arc location looks like Fig. 4, where z_0 denotes an arbitrary position of interest. This is the characteristic of the effect of arc on the weld width and the depression.

The arc is actually an integration of the arc length and welding current. Therefore, one can consider $(z_0^{(2)}, z_0 + (z_0 - z_2))$ as a geometrical integration of the effect intervals of both the arc length and welding current on the weld width rather than simply the effect interval of arc length or of welding current on the weld width. A similar interpretation can be made for $(z_0^{(1)}, z_0 + (z_0 - z_1))$.

3 Mathematical Description

Suppose the view shown in Fig. 3 is obtained at the kth sampling instant. At this instant, the laser stripe lies at z_3 (see Fig. 3). Let us define: (1) the weld width and the depression at z_3 by $h(k)$ and $b(k)$, respectively, and (2) the welding current and arc length at this instant, corresponding to the arc positioned at z_0 (see Fig. 3), by $i(k)$ and $l(k)$, respectively.

Choose z_3 so that d_1 is a positive integer where d_1 is given by

$$d_1 = (z_1 - z_3)/TV$$

where T is the sampling period and V is the torch velocity. Suppose L denotes the set of positive integers. Then, we can define M_1, d_2, and M_2 by the following:

$$M_1 = \min L(L : LTV \geq (z_0 + (z_0 - z_1)) - z_0^{(1)}) \quad (1)$$

$$d_2 = \max L(L : LTV \leq z_2 - z_3) \quad (2)$$

$$M_2 = \min L(L : LTV \geq ((z_0 + (z_0 - z_2)) - z_0^{(2)}) + ((z_2 - z_3) - d_2TV)) \quad (3)$$

Thus, we can obtain:

$$\begin{cases} h(k) = f_1(i(k - M_1 - d_1), \ldots, i(k - d_1), \\ \qquad l(k - M_1 - d_1), \ldots, l(k - d_1)) \\ b(k) = f_2(i(k - M_2 - d_2), \ldots, i(k - d_2), \\ \qquad l(k - M_2 - d_2), \ldots, l(k - d_2)) \end{cases} \quad (4)$$

where f_1, f_2 are notations of functional relationships.

It can be seen that d_1 and d_2 basically correspond to the delays of depression and weld width to the arc action, respectively. Similarly, M_1 and M_2 essentially correspond to the effect intervals of arc on depression and weld width, respectively. In fact, if the inequalities in (1) to (3) are changed to equalities, the previous relationships would be exact. Moreover, because both the arc length and welding current are included in the arc, the delay due to the arc length will, in general, be different from the delay due to the welding current. Similarly, the effect intervals of arc length and of welding current are also different. Thus, we define:

d_{11}: delay of h to i,

d_{12}: delay of h to l,

d_{21}: delay of b to i,

d_{22}: delay of b to l,

M_{11}: effect interval of i to h,

M_{12}: effect interval of l to h,

M_{21}: effect interval of i to b,

M_{22}: effect interval of l to b.

Using the definitions given above, the following equations can be obtained:

$$\begin{cases} h(k) = f_1(i(k - M_{11} - d_{11}), \ldots, i(k - d_{11}), \\ \qquad l(k - M_{12} - d_{12}), \ldots, l(k - d_{12})) \\ b(k) = f_2(i(k - M_{21} - d_{21}), \ldots, i(k - d_{21}), \\ \qquad l(k - M_{22} - d_{22}), \ldots, l(k - d_{22})) \end{cases} \quad (5)$$

In Eq. (5), M_{ij} and d_{ij} ($i = 1, 2, \quad j = 1, 2$) are the suborder and the subdelay of the system, respectively. Since the distances from z_1 to z_0 and z_2 to z_0 are affected by the weld pool size, d_{ij} and M_{ij} are actually influenced by the weld pool size as well. This produces uncertainty in the order and delay of the model.

It is well known that the weld width varies linearly with the welding current. Also, a linear model can be employed to describe the relationship between the back-side width and welding current for full penetration GTAW [16]. Thus, a linear relationship between our depression and the welding current can be assumed because of the linear relationship between the back-

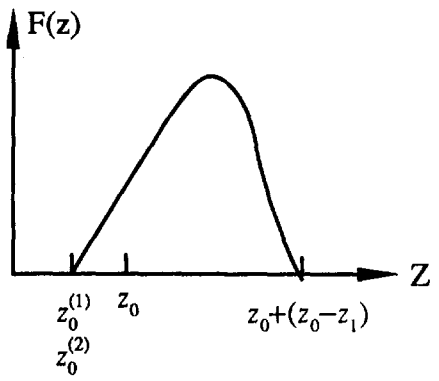

Fig. 4 Effects of arc on weld geometry at z_0 versus arc position

side width and our depression [1]. Regarding the effect of arc length on weld parameters, linear relationships have been suggested by our experiments. Thus, the following moving-average (MA) model is considered:

$$\begin{bmatrix} h(k) \\ b(k) \end{bmatrix} = \begin{bmatrix} b_{10} \\ b_{20} \end{bmatrix} + B \begin{bmatrix} i(k) \\ l(k) \end{bmatrix} + \begin{bmatrix} \epsilon_1(k) \\ \epsilon_2(k) \end{bmatrix} \tag{6}$$

where

$$B = \begin{bmatrix} \sum_{j=1}^{M_{11}} b_{11}(j) z^{-j-d_{11}} & \sum_{j=1}^{M_{12}} b_{12}(j) z^{-j-d_{12}} \\ \sum_{j=1}^{M_{21}} b_{21}(j) z^{-j-d_{21}} & \sum_{j=1}^{M_{22}} b_{22}(j) z^{-j-d_{22}} \end{bmatrix} \tag{7}$$

z^{-1} is the backshift operator, and $\epsilon_1(k)$ and $\epsilon_2(k)$ are independent white noise sequences. We note that from the standpoint of decreasing the number of parameters for on-line estimation in adaptive control, a model with an autoregression term is preferred. However, it has been found that the k-step-ahead accuracy of ARMA models decrease significantly with k. In the range of interest for our long-range predictive control, the accuracies associated with the above MA models are much better than the ARMA models. Thus MA models are selected.

4 Dynamic Experiments

4.1 Experimental Setup. The experimental setup is shown in Fig. 1. A Nd:YAG laser of 1.06 μm wavelength and an optical lens produce the structured-light plane. A narrow band optical filter with 123 Å half width together with a CCD camera is used to obtain the structured-light three-dimensional image of weld with a laser-stripe. The image is sampled and transformed into a 512 × 512 × 8 bits digital grey scale matrix by a frame grabber. The corresponding resolutions are $pixel_x$ = 0.05 mm and $pixel_y$ = 0.0436 mm along the x axis and y axis, respectively. The sampling and transforming are performed in real time. The image processing algorithm runs at 5 Hz. The welding equipment consists of a constant current rectified ac power supply, with a range of 60 amps to 350 amps, and an air cooled GTAW torch operating in a dc electrode negative mode. The welding current instruction is set by the computer through a 12 Bit D/A converter. For our dynamic experiments, the instructions for both the welding current and the arc length are preprogrammed. All of the computation (including giving input instruction, sampling and transforming the image, processing the digital grayness matrix and storing the computed results, $h(k)$ and $b(k)$), are performed in real-time.

Table 1 Typical welding conditions

No.	Position	Gap	Flow[1]	Condition [2]	θ
1	Bead-on-plate	No	15 l / min	Normal	30°
2	Butt	Natural	15 l / min	Normal	30°
3	Butt	0.5mm	15 l / min	Normal	30°
4	Butt	Natural	Varying	Normal	30°
5	Butt	Natural	15 l / min	Control	30°
6	Butt	Natural	15 l / min	Normal	45°

1 : Rate of argon flow. 2 : Heat transfer condition. θ: electrode tip angle.

4.2 Experimental Design. The time period is chosen to be 100 seconds based on the length of the experimental test-pieces and the torch velocity. The sampling period is selected to be 0.5 second according to the rule T_{95}/T = 5~15 where T_{95} is the 95 percent settling time of a transient process [24]. In our case, T_{95} of the response of h to step i is 4~6 seconds. Preliminary experiments have been performed to determine the operating point and the permitted range. The results are: the operating point–i_0 = 120A, l_0 = 3 mm; the permitted range–105$A \le i \le$ 135A, 1 mm $\le l \le$ 5 mm. At the operating point, full penetration welds with moderate back-side bead widths can be produced. Also, when the inputs vary around the operating point in the permitted range, the welds will be fully penetrated and no burn-through will occur. Therefore, the welds can be used for the dynamic analysis. Thus, the experimental inputs can be designed based on the acquired operating point and permitted range. In order to excite the process dynamics [24], the inputs should be varied. The resultant experimental inputs are plotted in Fig. 5.

4.3 Experimental Conditions. Experiments under six typical welding conditions are considered. These typical conditions are acquired by adding disturbances to the basic welding conditions. For each piece of experimental data, an individual mathematical model can be fitted. For all the experimental data, a general model, or said nominal model, is obtained to describe the general characteristics of the process. Table 1 shows the six typical welding conditions.

All the weldments are Type 321 austenitic stainless steel and have dimension of 100 millimeters in width, 250 millimeters in length, and 3 millimeters in thickness. The electrode is 2 percent thoriated tungsten with a diameter of 3 millimeters. The

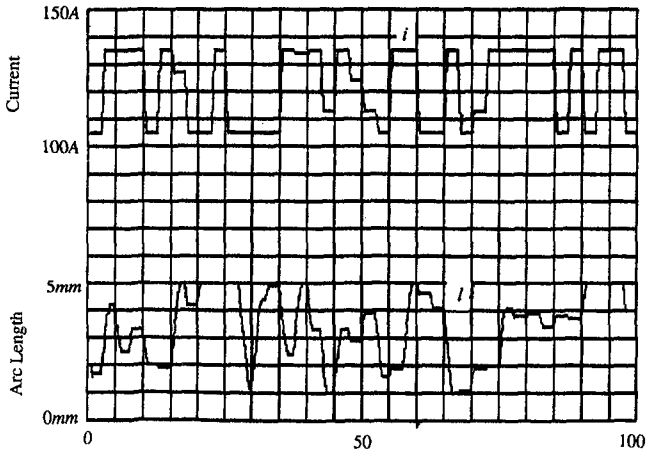

Fig. 5 Experimental inputs. The variations in the inputs are used to excite the dynamics of the process. The current and arc length are uncorrelated.

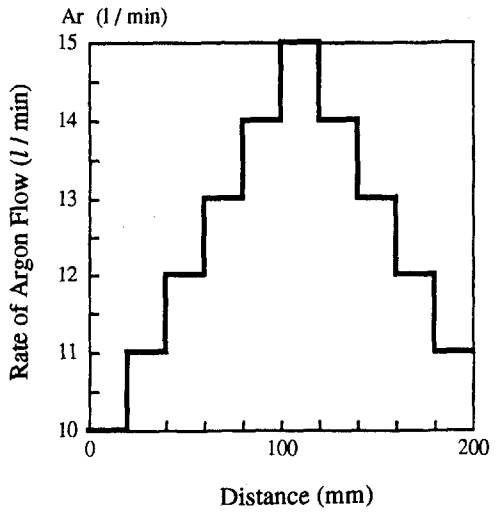

Fig. 6 Flow rate of shielding gas in Experiment 4

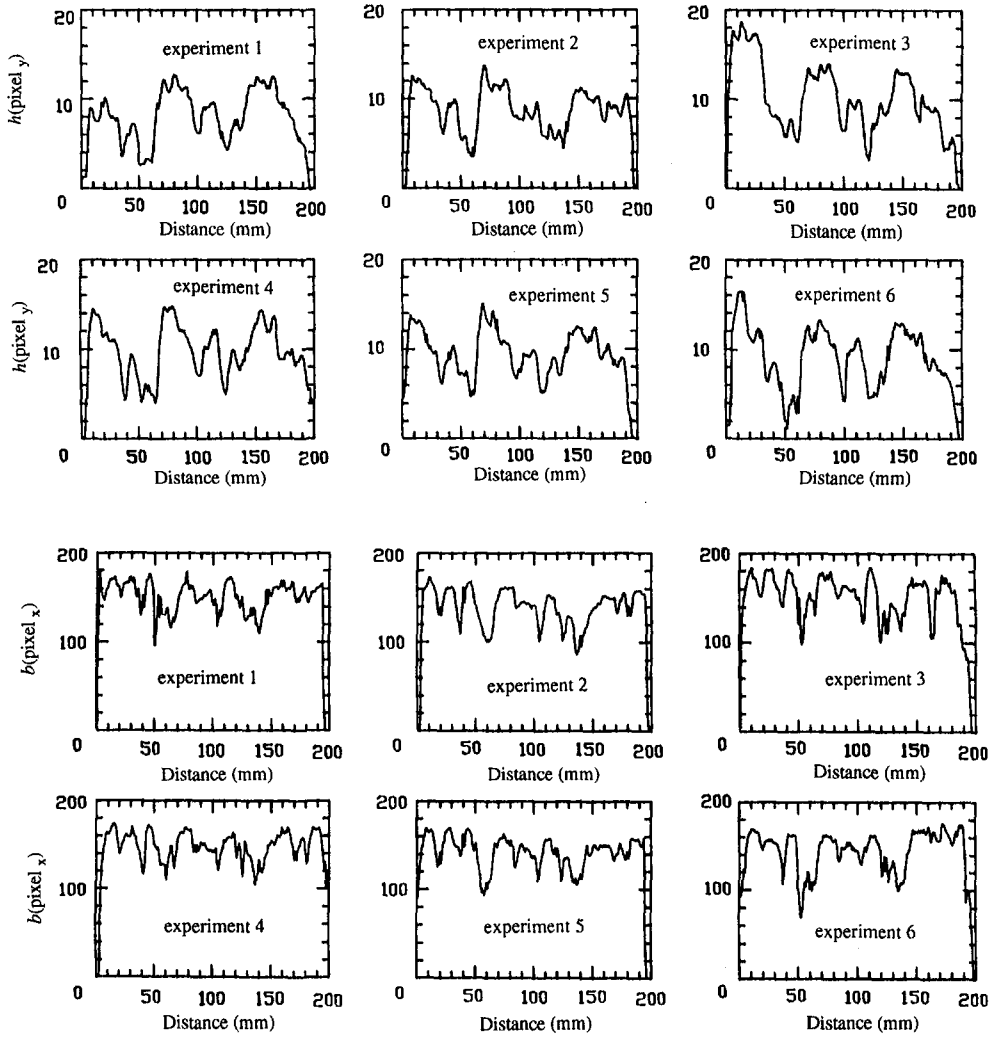

Fig. 7 Outputs of dynamic experiments. The similarity in the output waveforms among different experiments is caused by the inputs. The variations in the output values among different experiments shows that the outputs are also determined by the welding conditions.

torch velocity is 2 millimeters per second. High purity argon gas is employed as shielding gas.

In Table 1, the description "natural gap" for the gap between two plates to be joined is used. This description simply means that these two plates are slit and then directly placed together for butt welding. In Experiment 4 the flow rate of shielding gas varies as shown in Fig. 6. In Experiment 5 the heat transfer condition is disturbed by drilling holes on the plate and by insertion of asbestos cloth between the weldment and the fixture.

Figure 7 shows the outputs of the dynamic experiments.

5 Off-Line Modeling

Parameter Estimation is conducted by the least squares method [25]. Orders are determined by the *F-test* ($\alpha = 0.05$) [25]. Values of both the welding current and arc length appearing in the mathematical model are given by the differences between the actual values and the operating point.

5.1 Individual Models. Parameters of the resultant MA models are shown in Table 2. Note that the prediction error is independent of the prediction step. From Table 2 we observe that for different individual models, the orders, delays, $b_{ij}(k)$, b_{i0} and static gains ϕ_{ij} are generally distinct. These distinctions are intentionally retained to simulate the differences among the various welding conditions.

5.2 General Model. In order to obtain the general model, $h'(k) = h(k) - b_{10}$ and $b'(k) = b(k) - b_{20}$ are first calculated using corresponding individual b_{10} and b_{20} listed in Table 2. Then $h'(k)$ and $b'(k)$ of all the six experiments are employed to identify an unique B. The result is:

$$\begin{aligned} h'(k) = {} & -0.3845l(k-16-1) + 0.0364i(k-9-1) \\ & + 0.0107i(k-9-2) + 0.0214i(k-9-3) \\ & + 0.0064i(k-9-4) + 0.0075i(k-9-5) \\ & + 0.0318i(k-9-6) + 0.0240i(k-9-7) \\ & + 0.0406i(k-9-8) + 0.0149i(k-9-9) \\ & + 0.0120i(k-9-10) + 0.0221i(k-9-11) \\ & + 0.0175i(k-9-12) + 0.0377i(k-9-13) + \epsilon_1(k) \\ b'(k) = {} & 4.17l(k-17) + 0.3648i(k-15-1) \\ & + 0.1819i(k-15-2) + 0.1600i(k-15-3) \\ & + 0.1632i(k-15-4) + 0.0564i(k-15-5) \\ & + 0.2155i(k-15-6) + \epsilon_2(k) \end{aligned} \quad (8)$$

where the variances of ϵ_1 and ϵ_2 are 1.200^2 pixel$_y^2$ and 9.193^2 pixel$_x^2$, respectively.

Table 2 Identified model parameters

	No.	d_{11}	d_{12}	M_{11}	M_{12}	b_{10}	b_{11} (10^{-2})	b_{12}	ϕ_{11}	ϕ_{12}	σ
depression subsystem	1	7	13	11	1	8.00	3.3, 0.6, 4.2 0.1, 0.9, 1.0, 4.9, 0.4 3.2, 2.0, 6.0	-0.32	0.31	-0.32	1.29
	2	10	21	11	1	8.37	5.2, 0.8, 0.8, 1.3, -5.9, 1.5 1.3, 1.4, -0.2, 5.1, -0.1	0.25	0.23	0.25	1.46
	3	10	15	9	1	9.24	5.3, 1.3, 1.7, 2.4, -0.5, 3.2 1.4, 1.1, 5.2	-0.75	0.22	-0.75	1.62
	4	10	15	13	1	9.63	3.2, -0.3, 1.3, 1.1, 2.7, 4.7 2.2, 3.9, 1.9, 2.0, 4.0,1.2, 3.5	-0.48	0.32	-0.48	1.12
	5	7	11	11	1	9.45	4.3, 0.3, 0.2, 0.3, 1.0, 4.8 0.6, 1.3, 2.2, 2.5, 5.6	-0.38	0.23	-0.38	1.33
	6	9	15	11	1	9.04	6.0, 0.6, 1.1, 0.7, 1.1, 6.3, 7.5 1.9, 2.1, 1.7, 8.3	-0.55	0.31	-0.55	1.76
	No.	d_{21}	d_{22}	M_{21}	M_{22}	b_{20}	b_{21}	b_{22}	ϕ_{21}	ϕ_{22}	σ
weld width subsystem	1	17	11	8	1	146.3	0.318, 0.156, 0.297, -0.011 0.049, 0.220, 0.275, -0.114	4.54	1.17	4.54	10.33
	2	16	16	3	1	134.9	0.331, 0.259, 0.419	5.19	1.01	5.19	13.06
	3	15	11	2	1	150.6	0.378, 0.297	4.06	0.66	4.06	16.09
	4	16	17	3	1	145.2	0.272, 0.181, 0.440	4.46	0.89	4.46	9.19
	5	15	15	2	1	137.8	0.416, 0.426	5.59	0.84	5.59	11.34
	6	13	12	9	1	140.9	0.286, 0.183, 0.210, 0.251 0.091, 0.240, 0.187, 0.108, 0.190	5.12	1.75	5.12	13.44

ϕ_{ij}(i=1, 2; j=1, 2): Static gain. σ : Root variance.

6 On-Line Modeling

Significant differences exist between the parameters in different models. The best *a priori* knowledge of the process is the general model. An inaccurate model is therefore encountered by the control algorithm. The control performance will be influenced. To improve control quality, an adaptive control where the parameters of the control algorithm are on-line adjusted based on the on-line updated process model is preferred. Thus, the on-line model modification needs to be studied.

The model modification method should be selected. There are two possible methods: (1) modify all the parameters in MA models on-line, excluding the structure parameters M_{ij} and d_{ij} (2) modify a few key parameters on-line. In most other self-tuning control applications the first method is adopted. However, in our case, the number of parameters in the MA model is large and the **duration of the process is short** (only 200 sampling instants). Therefore, only a few key parameters can be identified on-line.

In order to select the key parameters, let us first present the following preliminary real time model (PRTM):

$$\begin{cases} h(k) = b_{10} + h'(k) \\ b(k) = b_{20} + b'(k) \end{cases} \tag{9}$$

where h' and b' are described in (8) and reflect the general characteristic of the process, and the base values b_{10} and b_{20} depend on the welding conditions. Obviously, if such a model is taken as our real time dynamic model, the key parameters b_{10} and b_{20} can be easily identified on-line.

In order to investigate the effectiveness of our PRTM as a real time model, we can take the values of b_{10} and b_{20} as given in Table 2, and then obtain an open-loop prediction. The comparison between the measured values and the predicted values has shown that the open-loop prediction result is satisfactory. However, this comparison does not faithfully reflect the practical effectiveness of PRTM in that b_{10} and b_{20} are not known during actual welding. If we suppose the mathematical model does not vary during a particular welding, the estimate of base values will rapidly converge to their actual values. In this case, the effectiveness will be nearly the same as that of the comparison. If b_{10} and b_{20} vary during welding, the effectiveness of multistep ahead prediction cannot be shown by the comparison even if the estimate of b_{10} and b_{20} can converge to their true values as soon as possible, since we do not predict b_{10} and b_{20} ahead of time. In this case, how much the comparison can reflect the prediction effectiveness of PRTM will primarily depend on the variation of b_{10} and b_{20} relative to the prediction step.

As system parameters, the variations of both b_{10} and b_{20} are probably due to inaccuracies of our model structure and the change in welding conditions along the weld seam. The change in welding conditions is in general slow, for instance, the change of heat transfer condition along the weld seam caused by weldment structure. Consequently, the resultant change of both b_{10} and b_{20} is slow as well. Thus the welding conditions do not influence greatly the effectiveness of our PRTM.

The above discussion shows that for the PRTM, when the welding conditions do not quickly vary relative to the prediction step, a more accurate prediction can be obtained by means of identifying b_{10} and b_{20} in real-time. To improve the model further, the gain of the system can also be on-line identified. Thus, the following frame is proposed as the real time model.

$$\begin{cases} h(k) = b_{10} + \lambda_1 h'(k) \\ b(k) = b_{20} + \lambda_2 b'(k) \end{cases} \tag{10}$$

where λ_1 and λ_2 are the so-called gain modification coefficients. This real-time model frame better incorporates the general characteristic (described by h' and b') to h and b which are encountered during actual welding. Its parameters, i.e., b_{j0} and λ_j (j = 1, 2), can easily be on-line identified.

The on-line identification results of the real-time model parameters are plotted for the typical welding conditions (Fig. 8). It is seen that the parameters vary along the weld seam, although the change is not very fast. These variations are caused by the variation of the practical welding conditions along the seam. The influence of these variations on the model can, therefore, be tracked by the on-line identified model parameters. To show

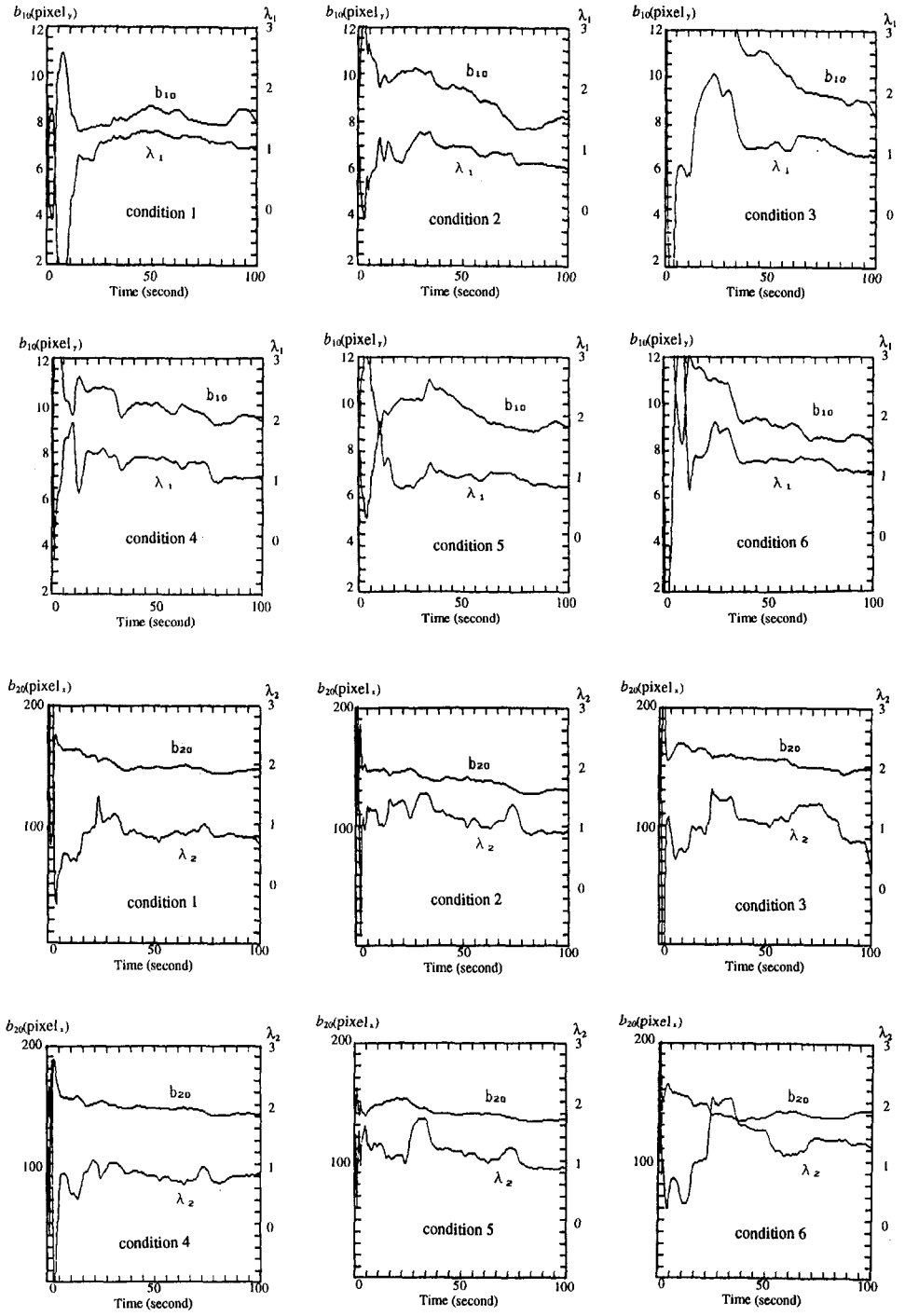

Fig. 8 On-line identification of real-time model parameters. The variations in the parameters among different conditions are caused by the variations in welding condition. The variations along the weld seam shows that variations in welding condition exists along the seam.

the accuracy of the on-line identified model, the on-line identified parameters can be used to predict the process outputs. If the predicted outputs are close to the measured outputs, the identified real-time model can be regarded as being accurate. In Fig. 9, the predicted outputs using the on-line identified real-time model are plotted in addition to the measured outputs. It is evident that the error between predicted and measured outputs is very small. Thus, the proposed real-time model frame is acceptable.

The real-time model is also shown to be sufficient for our control problem by simulations of predictive control where the six typical welding conditions are emulated by the individual models and the real-time model is utilized by the controller. The results are plotted in Fig. 10. For comparison, the simulation results of predictive control without utilization of the real-time model are given in Fig. 11. It can be seen that noticeable errors exist in Fig. 11. This is caused by the slow identification speed associated with a high order model. It is apparent that the real-time model significantly improves the effectiveness of the adaptive predictive control.

7 Process Characteristics

The process characteristics play a primary role in selecting the control algorithm. In this section, the process charac-

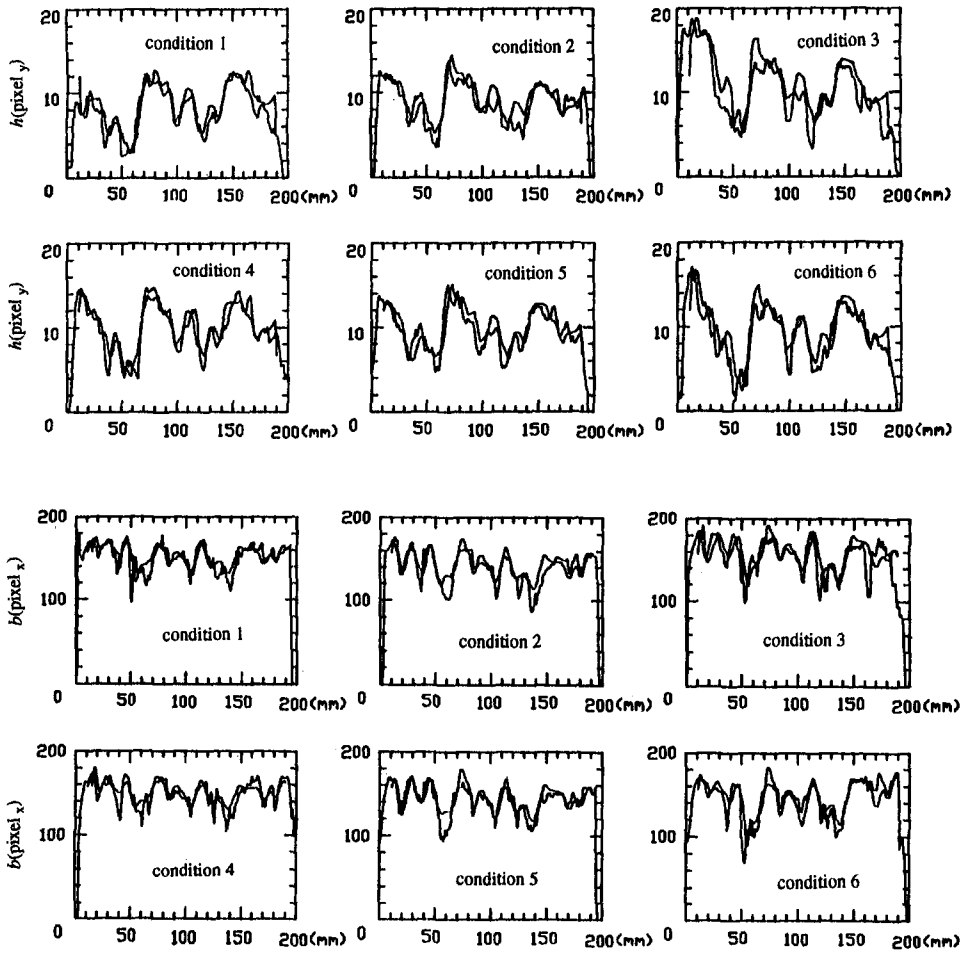

Fig. 9 Predicted outputs using the on-line identified real-time model. Two curves are plotted in each drawing. One is the predicted output. Another is the measured output. Attention should be paid to the difference between the two curves which illustrates the model error. It can be seen that observed model error is very small.

teristics will be discussed based on the acquired dynamic models.

7.1 Inertia. The inertia are determined primarily by M_{ij} and, to a less extent, by $b_{ij}(k)$ $(i = 1, 2, j = 1, 2; k = 1, \ldots, M_{ij})$. The larger M_{ij} is, the greater the corresponding inertia. Depending on M_{ij} $(i = 1, 2; \quad j = 1, 2)$, the inertia are divided into four categories: (1) depression to welding current (M_{11}); (2) depression to arc length (M_{12}); (3) weld width to welding current (M_{21}); (4) weld width to arc length (M_{22}). The following can be seen from Eq. (8): (1) Both the depression to arc length inertia and the weld width to arc length are small because both M_{12} and M_{22} are unity; (2) Both the depression to welding current and the weld width to welding current inertia are large because $M_{21} = 6$ and $M_{11} = 13$. However, the depression to welding current inertia is much larger than the weld width to welding current inertia.

The proceeding results on process inertia can be understood via analysis of the welding process. In fact, the majority of the heat input into the weldment is primarily determined by the welding current and little depends on the arc length. This is because a change in arc length produces only a variation in the voltage drop of the arc volume while the voltage drop of the arc spot is basically constant. Thus, for the positions where the arc is not directly aimed, the effect of arc length is negligible since the arc acts primarily through heat transfer rather than force transfer and the influence of arc length on the power of the heat input is small. Accordingly, the inertia of the weld geometrical parameters (including depression and weld width) to arc length is small. Of course, due to the travel of arc and the delays, the position where the arc achieves the maximum effect on the weld formation is not the position corresponding to the arc center but a position slightly behind the center. Additionally, the reason why the weld width to welding current inertia is smaller than the depression to welding current inertia is that the fixed position of the weld width (z_2) is closer to the arc than the position of the depression (z_1) is to the arc (see Fig. 3).

7.2 Delays. For our process, the main causes of delays are the distances between the sampling position z_3 to both z_2 and z_1, and the travel of the arc. Because $z_1 - z_3 \gg z_2 - z_3$, the delays of the weld width are much larger than the delays of the depression. In fact, from (8) we have seen that $d_{11} = 9$, $d_{12} = 16$, $d_{12} = 15$, $d_{22} = 16$.

We remark that the delays in mathematical models are simply estimates. Actually, after the distance between z_3 and z_0 has been fixed, the delays will depend directly on the weld pool size due to the effect of weld pool size on z_2 and z_1. When disturbances exist or the inputs vary, the weld pool size will change. As a result, the delays will vary also. Therefore, during actual welding, the delays are uncertain and the values of delays in (8) are the estimates of the delays for the six typical experiments.

Based on the discussion, we conclude that (1) the delays are uncertain or varying; (2) different types of delays assume distinct values; (3) the delays of weld width are quite large since the sampling is performed just behind the end of the weld

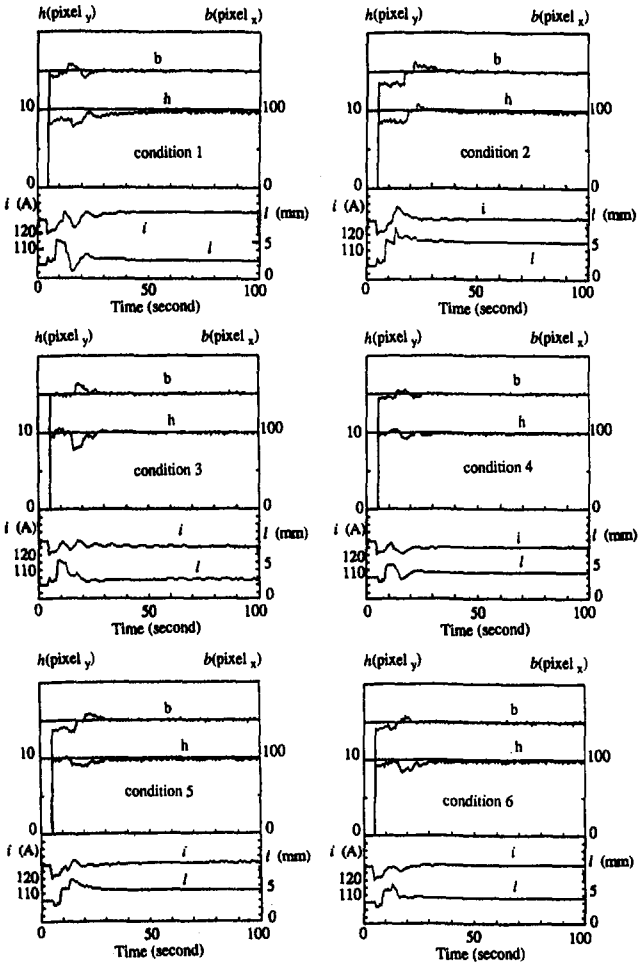

Fig. 10 Predictive control simulations using the real-time model

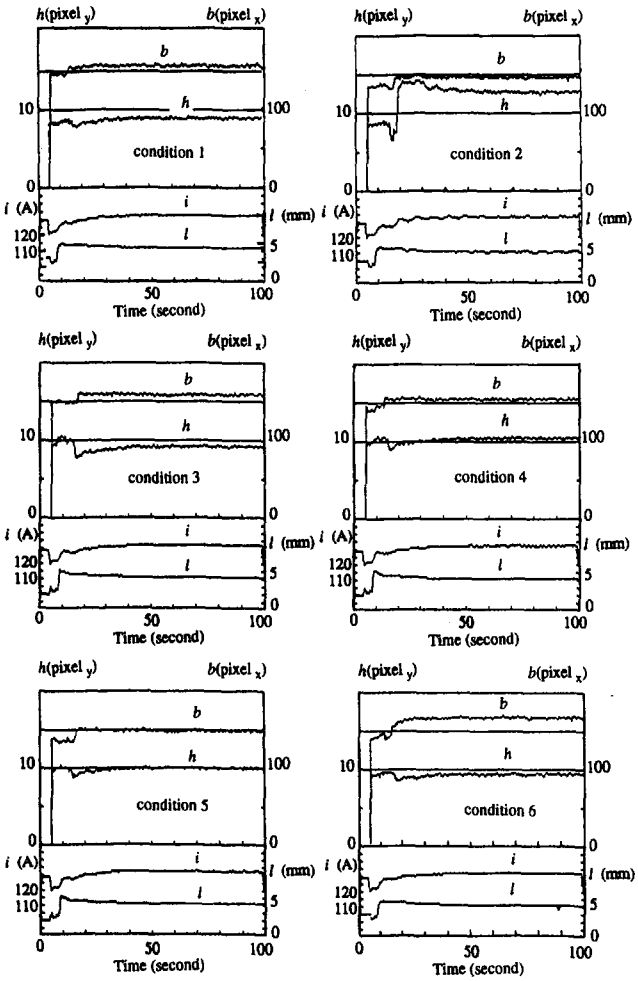

Fig. 11 Predictive control simulations without the real-time model

pool, which is distant from the position where the weld width is fixed.

7.3 Nonminimum Phase. An investigation into (8) reveals that the depression subsystem is nonminimum phase [13] due to zeros lying outside the unit circle.

7.4 Coupling. A decoupling control is frequently preferred to other multivariable controllers for many practical control problems. In order to realize a decoupling control, the input-output pairing relationship should be determined.

It is well known that the depression is mainly affected by the welding current, and the weld width is primarily affected by the arc length. However, the mathematical model (8) shows the strong effect of welding current on the weld width. Thus, the Bristol-Shinskey method [26] is employed.

The static gain matrix Φ is:

$$\Phi = \begin{bmatrix} \phi_{11} & \phi_{12} \\ \phi_{21} & \phi_{22} \end{bmatrix} = \begin{bmatrix} 0.0984 & -0.3845 \\ 0.4060 & 4.1700 \end{bmatrix}$$

The relative gain matrix Λ can be calculated accordingly:

$$\Lambda \triangleq \Phi^* [\Phi^{-1}]^T \triangleq \begin{bmatrix} \lambda_{11} & \lambda_{12} \\ \lambda_{21} & \lambda_{22} \end{bmatrix} = \begin{bmatrix} 0.72 & 0.28 \\ 0.28 & 0.72 \end{bmatrix}$$

where "*" means the following operation:

$$\Lambda_{ij} = \Phi_{ij} [\Phi^{-1}]_{ij}^T$$

where λ_{11} is the relative gain of the depression to the welding current, λ_{12} is the relative gain of the depression to the arc length, λ_{21} is the relative gain of the weld width to the welding current, and λ_{22} is the relative gain of the weld width to the arc length. Therefore, we should choose the input-output pairing relationship: $i \sim h$, $l \sim b$. Meanwhile, since the relative gain of coupling path is 0.28, an obvious coupling between output and operative variable can be observed (see Fig. 12).

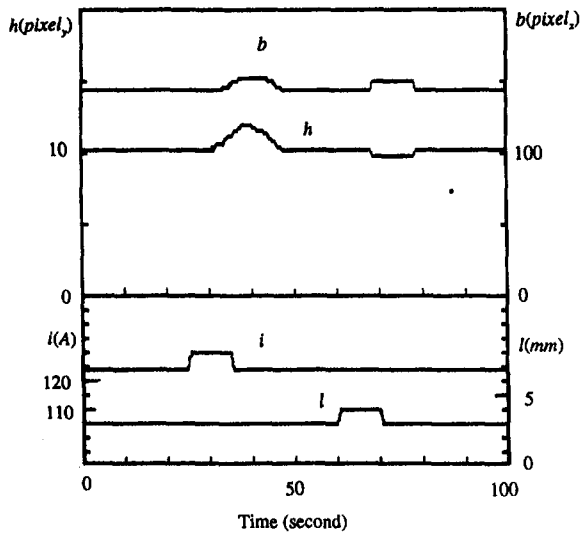

Fig. 12 Coupling observation

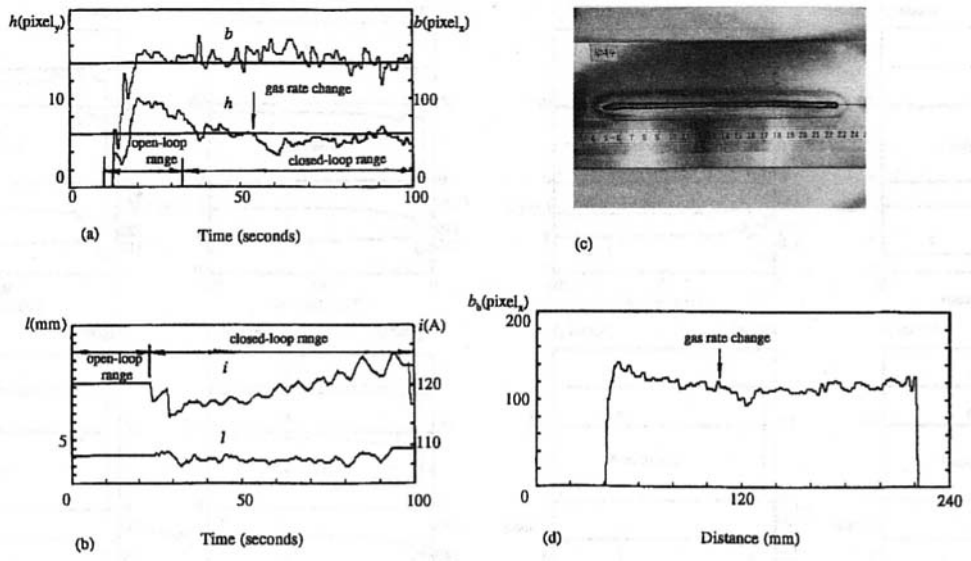

Fig. 13 Closed-loop control under gas rate variation. The larger initial current makes h larger during the initial open-loop control period. h is quickly adjusted to the desired level after the closed-loop control begins. At t = 53 seconds, the gas rate is changed from 10 l/min to 5 l/min. Thus, h decreases. The feedback controller increases the current accordingly. Hence, h returns to the desired level again. (*a*) on-line measured top-side parameters (*b*) control actions (*c*) back-side photograph of the workpiece (*d*) off-line measured b_b

8 Control

The acquired process characteristics and models will be used to develop the final control system in this section.

8.1 Algorithm Selection. It has been seen that the process model depends on the welding condition. Inexact orders and delays will be encountered. For such a type of process, conventional adaptive algorithms such as the generalized minimum variances (GMV) or pole-placement will probably fail [11]. For example, the GMV performs poorly if the delay varies, even if it is robust with respect to our assumed model order. Other approaches which attempt to estimate the delays using operating data tend to be complex and lack robustness [11]. Unless special precautions are taken pole-placement and LQG self-tuner are sensitive to the overestimation of the model order due to the pole/zero cancellations in the identified model. To investigate the possibility of applying a multivariable PID or fuzzy controller, extensive simulations have been done. It was observed that their performance in terms of compromise between the response speed and overshooting was too poor to be accepted.

The generalized predictive control (GPC) presented by Clarke et al. [11] has been shown to be capable of effective control of a process simultaneously with variable delay, variable order and nonminimum-phase as well as open-loop unstable properties. This algorithm seems to be the most promising for our problem. Thus, adaptive GPC was selected. Also, due to the coupling, a decoupling algorithm has been incorporated with the predictive control algorithm. The resultant algorithm is an adaptive decoupling predictive control.

8.2 Algorithm Design and Implementation. The controller consists of the predictive control algorithm and predictive decoupling algorithm [27]. The predictive decoupling algo-

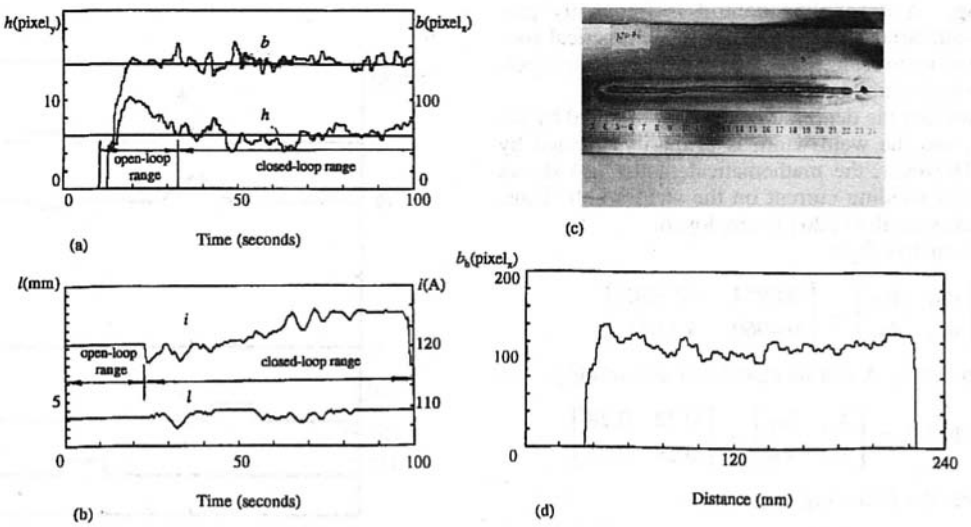

Fig. 14 Closed-loop control under gap variation. In the closed-loop control range, h and b_b are maintained at the desired level despite the varied gap. The current adaption to the varied gap can be observed from the control actions. (*a*) on-line measured top-side parameters (*b*) control actions (*c*) back-side photograph of the workpiece (*d*) off-line measured b_b

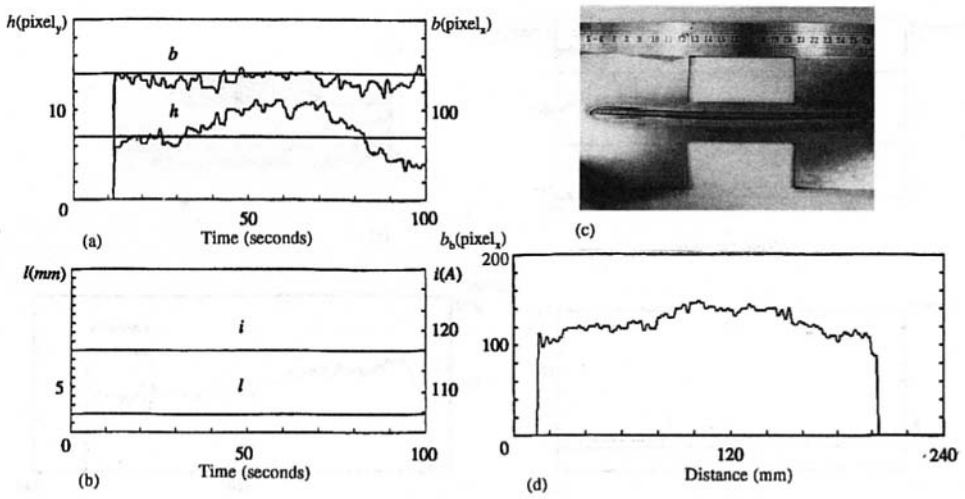

Fig. 15 Open-loop control under variation of heat transfer condition. Large variations in h and b_b are caused by the variation in heat transfer condition. (*a*) on-line measured top-side parameters (*b*) control actions (*c*) back-side photograph of the workpiece (*d*) off-line measured b_b

rithm is designed using the predictive optimization principle and the real-time model. The predictive control algorithm is designed based on the predictive control principle and the real-time model. The adjustable parameters, i.e., the smoothing factor, control action weight, etc. [11], are selected by simulation. In order to conduct simulations, individual models have been used to emulate the possible variations and disturbances. Thus, the control algorithm is designed and implemented using the acquired individual, general, and real-time models.

8.3 Closed-loop Control Experiments. The designed control algorithm has been used to conduct extensive closed-loop control experiments under varied heat transfer condition, electrode tip angle, butt root opening, and flow rate of shielding gas. These variations are used to emulate the stochastic or unexpected disturbances during welding which must be overcome by the closed-loop algorithm. The material, size, and thickness are the same as for the dynamic experiments. The torch speed is 2 mm per second. The control period is 0.5 second.

**Variation in the Rate of Shielding Gas Flow: θ = 60 deg*
This experiment is done to investigate the behavior of the system when a disturbance in shielding gas flow rate exists. Experimental results are shown by Fig. 13 where b_b, the back-side weld width, is measured off-line after the experiment. In this experiment, a step disturbance of shielding gas flow rate is applied (see the arrow in Fig. 13(a)) to change the rate from 10 l/min to 5 l/min).

Because of a 20 mm distance between the center of electrode and the laser stripe, the measurements of h and b are zero during the first 10 seconds (the time interval corresponding to 20 mm distance). Due to the delay from the arc strike to the formation of the weld bead, the actual interval of zero measurements of h and b is a little more than 10 seconds. Similarly, no measurements for the last 20 mm of the weld are taken and, therefore, cannot be indicated in Fig. 13(a).

In Fig. 13(a), a larger offset is observed during the starting period. This is caused by the difference between the actual model and the *a priori* model. This larger offset interval roughly

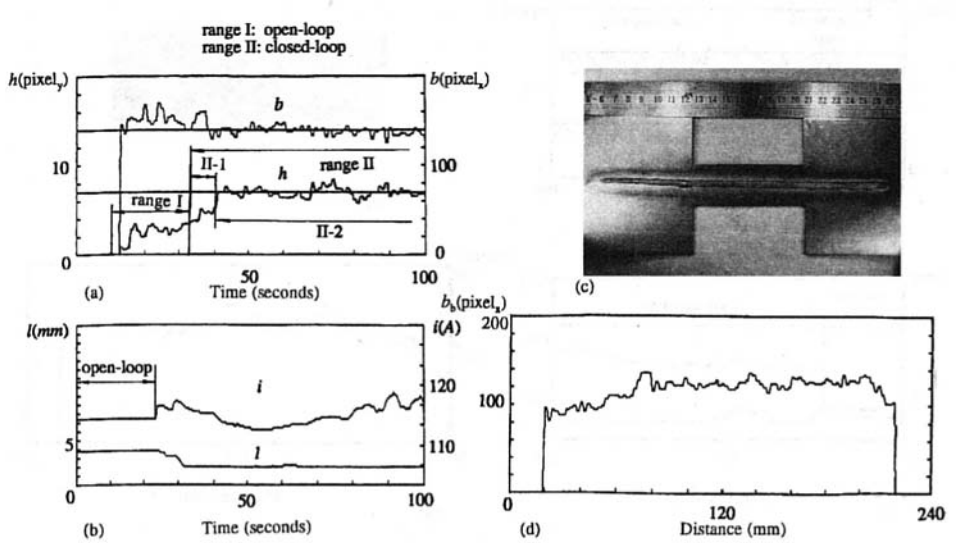

Fig. 16 Close-loop control under variation of heat transfer condition. Smaller initial current causes smaller h and b_b during the open-loop range. Once the closed-loop control begins, h and b_b quickly reach the desired levels. Then h and b_b are maintained at the desired levels despite the variation in heat transfer condition. The adaption can be seen from the current waveform. (*a*) on-line measured top-side parameters (*b*) control actions (*c*) back-side photograph of the workpiece (*d*) off-line measured b_b

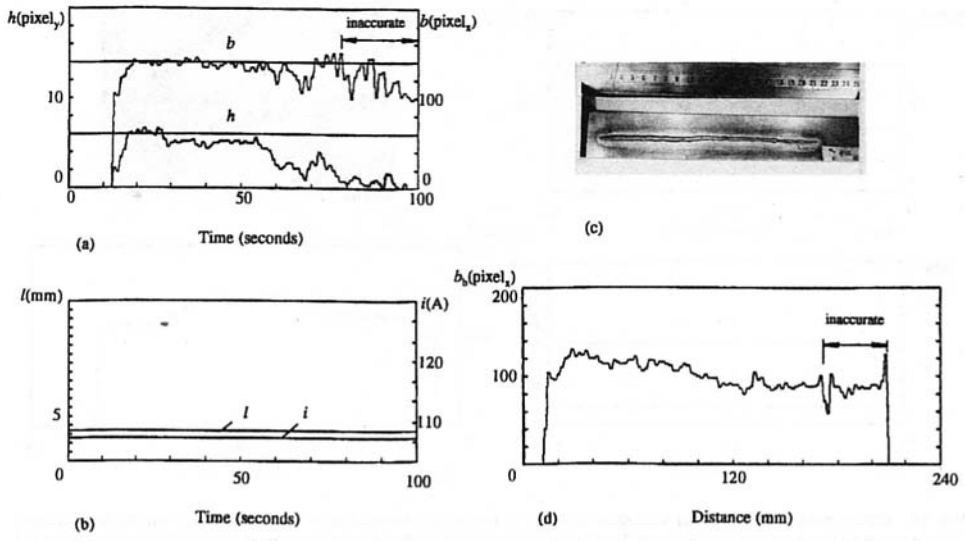

Fig. 17 Open-loop control under variation of gas rate and arc length. The arc length gradually changes from 3 mm to 4 mm. Before the gas rate is changed from 10 l/min to 5 l/min, slight decreases in h and b_b are observed. When the gas rate decreases, h and b_b are reduced severely. (a) on-line measured top-side parameters (b) control actions (c) back-side photograph of the workpiece (d) off-line measured b_b

corresponds to the initial welding parameters, which is calculated based on the *a priori* model. It is observed that when the feedback measurements are available, the correct control actions are taken at once (Fig. 13(a)). Despite the inherent large delay and the large offset, the performance of the control system is still very good.

It is known that the decrement of the rate of argon flow will reduce the effect of compression and cooling on the arc. Consequently, the arc will be decentralized. As a result, the parameters of the field of arc pressure are changed and the energy density of the arc volume decreased. This, in turn, increases the weld width slightly, and decreases the depression. However, through the measurements of both h and b, a proper corrective control action is taken, thereby maintaining h and b near the set-points. Therefore, the disturbance of the flow rate of shielding gas is overcome.

The final objective of our study is to control the back-side weld width b_b. As shown in Fig. 13(c) and (d), the control effectiveness for b_b is excellent.

**Variation in gap between two plates to be joined: θ = 60 deg* The gap between two plates to be joined varies from 0 to 0.5 mm gradually. The rate of argon flow is 10 l/min. The results are shown in Fig. 14. It can be seen that h and b are maintained near the set-points due to the regulation of control actions, especially the welding current. In fact, in most cases, the top-side weld width b is not sensitive to the disturbances in our experiments, unlike the depression h. Therefore, in most cases, a larger regulation of arc length is seldom observed except in the initial regulation period.

It can be seen that a good full penetration state has also been realized in the case of varying gap.

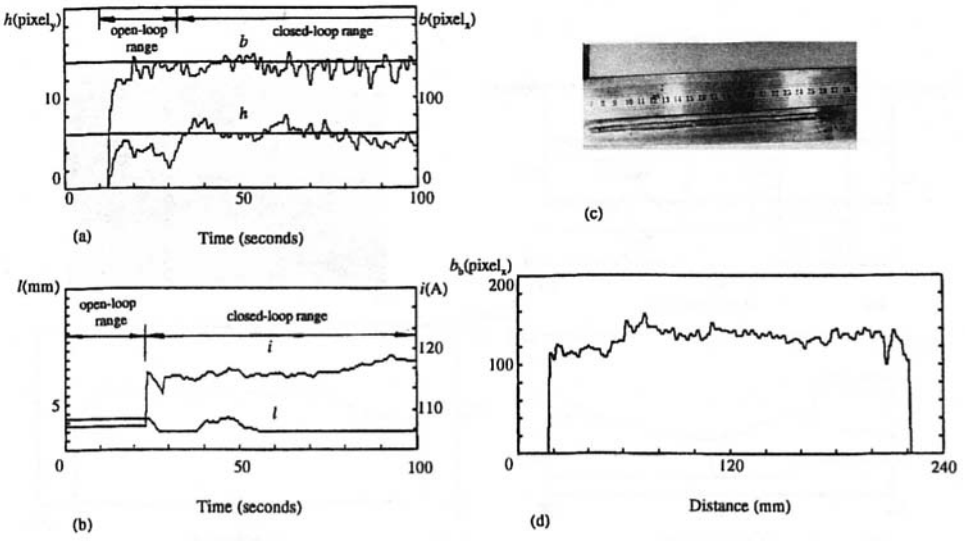

Fig. 18 Closed-loop control under variation of gas rate and arc length. The arc length and gas rate change as in the open-loop control experiment. In the open-loop range, h and b_b are smaller than the desired values. When the closed-loop control begins, the current increases rapidly. This makes h reach the desired level quickly. Then h is maintained at the desired level despite the variations in gas rate and arc length. (a) on-line measured top-side parameters (b) control actions (c) back-side photograph of the workpiece (d) off-line measured b_b

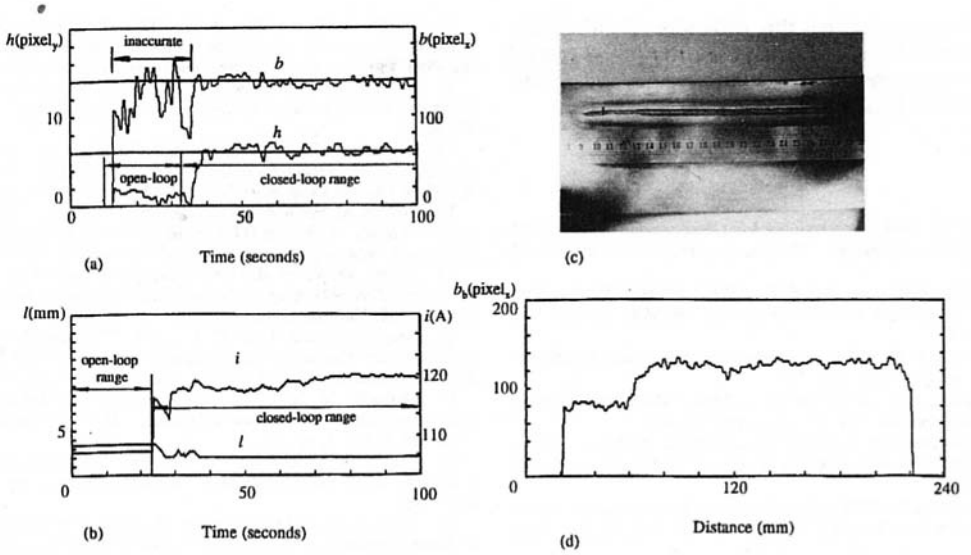

Fig. 19 Closed-loop control for electrode tip angle. A larger electrode tip angle is used than in the experiment of Fig. 18. This makes h much smaller than the desired level in the open-loop period. However, h reaches the desired level rapidly after the closed-loop control begins. (*a*) on-line measured top-side parameters (*b*) control actions (*c*) back-side photograph of the workpiece (*d*) off-line measured b_b

**Varying Heat Transfer Condition: θ = 60 deg* Varying heat transfer condition is emulated by the geometry of the test-piece (see Fig. 15(*c*)). In this case, the bead-on-plate is done. The rate of argon flow is 15 l/min. The open-loop and closed-loop results are shown in Fig. 15 and Fig. 16, respectively.

As can be seen from Fig. 15, under the varying heat transfer condition both b_b and h in the open-loop experiment are influenced by the heat transfer condition. However, in the case of the closed-loop, no influence of heat transfer condition on either h or b_b is observed (see Fig. 16). In fact, the waveform of i in Fig. 16(*b*) has exposed the adaption to the heat transfer condition.

In Fig. 15 the initial welding parameters are different from the experiments in Figs. 13 and 14 due to the larger disturbance from the heat transfer condition. If the initial welding parameters in Figs. 13 and 14 were used, h and b would become much larger. In addition, in the closed-loop experiment, the same initial welding parameters are used for the convenience of comparison.

**Step Change of the Rate of Argon Flow and Gradual Change of the Arc Length: θ = 45 deg* Both the open-loop and the closed-loop experiments have been performed under the same welding condition. In these two comparative experiments, the arc length varies from 3 mm to 4 mm gradually for no regulation, and a step change of the rate of argon flow from 10 l/min to 5 l/min takes place about 50 seconds after welding starts. The experimental results are shown in Fig. 17 and Fig. 18, respectively.

From Fig. 17 it can be observed that before the step change of the gas flow rate is applied the depression slightly decreases gradually. However, when the step change is applied, the depression decreases severely so that the measurements cannot be trusted due to the poor accuracy in the case of very small depression. Therefore, it can be seen that the state nearly achieves partial penetration from a good full penetration state under the disturbances of the rate and arc length. However, an excellent state is always maintained when the designed control system is used (see Fig. 18).

**Experiment for the Electrode Tip Angle: θ = 60 deg* All the experimental conditions and the initial welding parameters are the same as in the experiments shown in Figs. 17 and 18 except for θ = 60 deg. The experimental results are shown in Fig. 19.

It is observed that, although the initial welding parameters are the same as in Fig. 17 and Fig. 18, h and b_b are much less before regulation. Of course, according to the conclusions on the influence of the angle of electrode tip on the distribution of arc pressure and on the weld formation, the above results are easily understood because of the larger angle of electrode tip in this experiment. However, when regulated, the welding current increases immediately. As a result, the influence of the angle of electrode tip on the top-side weld parameters and the back-side weld width is overcome.

**Experimental Summary* It can be seen from the above experiments that the uniform back-side weld width can always be achieved despite different disturbances. It is evident that the analysis and identification play an important part in this achievement.

9 Conclusions

The current and arc length are selected to adjust the weld depression and width behind the weld pool rear in order to control the full penetration state in gas tungsten arc welding. The addressed process is defined by its inputs (current and arc length) and outputs (weld depression and width). The variations in heat transfer condition, electrode tip angle, butt gap, and rate of shielding gas are recognized as the process disturbances, while the torch velocity, plate thickness, material, and diameter of the electrode are recognized as being unchanged. These disturbances and unchanged welding conditions are used to design the experiments which generate data for the model fitting. It is shown by the fitted models that the model parameters, such as the orders, delays, and coefficients, significantly vary with the welding conditions. Also, the orders and delays are high. The process is found to be non-minimum phase. Because of these features, a qualified robust adaptive control algorithm is required. Thus, the adaptive generalized predictive control is selected. It is observed that a change in either the current or the arc length will generate variations in both the weld depression and weld width. This interaction is referred to as "coupling" in control design. Thus, for a practical application, a decoupling algorithm may be preferred. To realize the adaptive control, the model must be on-line identified. But, the welding duration is usually short. Because of the high orders, the on-line identification of the model will be difficult. The proposed

real-time model frame overcame this difficulty. Both simulations and experiments have shown that the designed control system based on the provided process characteristics and models is qualified for the full penetration state control.

References

1 Zhang, Y. M., et al., 1993, "Determining Joint Penetration in GTAW with Vision Sensing of Weld Face Geometry," *Welding Journal,* Vol. 72, No. 10, pp. 436s–469s.

2 Giedt, W. H., Wei, X.-C., and Wei, S.-R., 1984, "Effect of Surface Convection on Stationary GTA Weld Zone Temperatures," *Welding Journal,* Vol. 63, No. 12, pp. 376s–383s.

3 Kou, S., and Wang, Y. H., 1986, "Weld Pool Convection and Its Effect," *Welding Journal,* Vol. 65, No. 3, pp. 63s–70s.

4 Zacharia, T., Erslan, A. H., and Aidun, D. K., 1988, "Modeling of Autogenous Welding," *Welding Journal,* Vol. 67, No. 3, pp. 53s–62s.

5 Tekriwal, P., and Mazumder, J., 1988, "Finite Element Analysis of Three-Dimensional Transient Heat Transfer in GMA Welding," *Welding Journal,* Vol. 67, No. 7, pp. 150s–156s.

6 Tsai, M. C., and Kou, S., 1990, "Electromagnetic-force-induced Convection in Weld Pools with a Free Surface," *Welding Journal,* Vol. 69, No. 6, pp. 241s–246s.

7 Choo, R. T. C., Szekely, J., and Westhoff, R. C., 1990, "Modeling of High-Current Arcs with Emphasis on Free Surface Phenomena in the Weld Pool," *Welding Journal,* Vol. 69, No. 9, pp. 346s–361s.

8 Kim, S. D., and Na, S. J., 1992, "Effect of Weld Pool Deformation on Weld Penetration in Stationary Gas Tungsten Arc Welding," *Welding Journal,* Vol. 71, pp. 179s–193s.

9 Choo, R. T. C., and Szekely, J., 1994, "The Possible Role of Turbulence in GTA Weld Pool Behavior," *Welding Journal,* Vol. 73, pp. 25s–31s.

10 Kovacevic, R., Zhang, Y. M., and Ruan, S., 1995, "Sensing and Control of Weld Pool Geometry for Automated GTA Welding," ASME JOURNAL OF ENGINEERING FOR INDUSTRY, Vol. 117, No. 2, pp. 210–222.

11 Clarke, D. W., Mohtadi, C., and Tuffs, P. S., 1987, "Generalized Predictive Control," *Automatica,* Vol. 23, No. 2, pp. 137–160.

12 Kurz, H., and Goedecke, W., 1981, "Digital Parameter-adaptive Control of Processes with Unknown Dead Time," *Automatica,* Vol. 17, pp. 245–252.

13 Barthel, J. W., and Shin, Y. C., 1993, "Adaptive Control of Nonminimum Phase Processes with Application to the End Milling Process," *Proceedings of the 1993 American Control Conference,* San Francisco, CA, pp. 2449–2453.

14 Pietrzak, K. A., and Packer, S. M., 1994, "Vision-based Weld Pool Width Control," ASME JOURNAL OF ENGINEERING FOR INDUSTRY, Vol. 116, No. 1, pp. 86–92.

15 Schiano, J. L., Ross, J. H., and Weber, R. A., 1991, "Modeling and Control of Puddle Geometry in Gas Metal-arc Welding," *Proceedings of the 1991 American Control Conference,* June 26–28, Boston, MA, pp. 1044–1049.

16 Suzuki, A., Hardt, D. E., and Valavani, L., 1991, "Application of Adaptive Control Theory to On-line GTA Weld Geometry Regulation," ASME *Journal of Dynamic Systems, Measurement, and Control,* Vol. 113, pp. 93–103.

17 Nishar, D. V., et al., 1993, "Adaptive Control of Temperature in Arc Welding," *Proceedings of the Second IEEE Conference on Control Applications,* Sept. 13–16, Vancouver, B. C., Canada, pp. 948–952.

18 Song, J.-B., and Hardt, D. E., 1994, "Dynamic Modeling and Adaptive Control of the Gas Metal Arc Welding Process," ASME *Journal of Dynamic Systems, Measurement, and Control,* Vol. 116, No. 3, pp. 405–413.

19 Donnelly, M. K., et al., 1993, "Control of a Dynamic Brake to Reduce Turbin-generator Shaft Transient Torques," *IEEE Transactions on Power Systems,* Vol. 8, No. 1, pp. 67–73.

20 Eexter, A. L., and Haves, P., 1989, "A Robust Self-tuning Predictive Controller for HVAC Applications," *ASHRAE Transactions,* Vol. 95, Part 2, pp. 431–438.

21 Hogg, B. W., and El-Rabaie, N. M., 1990, "Generalized Predictive Control of Steam Pressure in a Drum Boiler," *IEEE Transactions on Energy Conversion,* Vol. 5, No. 3, pp. 485–492.

22 Patwardhan, A. A., and Edgar, T. F., 1993, "Nonlinear Model Predictive Control of a Packed Distillation Column," *Industrial and Engineering Chemistry Research,* Vol. 32, No. 10, pp. 2345–2356.

23 Burgardt, P., and Heiple, C. R., 1986, "Interaction between Impurities and Welding Variables in Determining GTA Weld Shape," *Welding Journal,* Vol. 65, pp. 150s–155s.

24 Isermann, R., 1980, "Practical Aspects of Process Identification," *Automatica,* Vol. 16, No. 5, pp. 575–587.

25 Wu, S. M., and Pandit, S. M., 1983, *Time Series and System Analysis with Applications,* John Wiley and Sons, New York, Chapter 2.

26 Liu, C. H., 1983, *General Decoupling Theory of Multivariable Process Control Systems,* Springer-Verlag.

27 Zhang, Y. M., et al., 1992, "Adaptive Predictive Decoupling Control of Full Penetration Process in GTAW," *Proceedings of the 1st IEEE Conference on Control Application,* pp. 938–943, Sept. 1992, Dayton, OH.